ADVANCED ENERGY MATERIALS
www.advenergymat.de

Photopolymerized Gel Electrolyte with Unprecedented Room-Temperature Ionic Conductivity for High-Energy-Density Solid-State Sodium Metal Batteries

*Pengchao Wen, Pengfei Lu, Xiaoyu Shi, Yu Yao, Haodong Shi, Hanqing Liu, Yan Yu, and Zhong-Shuai Wu**

Solid-state sodium metal batteries (SMBs) are highly promising rechargeable batteries owing to the abundance and cost effectiveness of sodium. However, the low room-temperature ionic conductivity and narrow voltage window of solid-state electrolytes seriously inhibit the development of SMBs. Herein, an ethoxylated trimethylolpropane triacrylate based quasisolid-state electrolyte (ETPTA–$NaClO_4$–QSSE) is developed by photopolymerization for high-energy-density solid-state SMBs. The ETPTA–$NaClO_4$–QSSE exhibits remarkable room-temperature ionic conductivity of 1.2 mS cm^{-1}, a wide electrochemical window of >4.7 V versus Na^+/Na, and excellent flexibility. Owing to outstanding interfacial compatibility between this electrolyte and the electrode, Na metal symmetrical batteries show ultralong cyclability with 1000 h at 0.1 mA cm^{-2}, and ultralow overpotential of 355 mV at 1 mA cm^{-2}, indicative of significant suppression of the Na dendrite growth. Notably, $Na_3V_2(PO_4)_3$ (NVP) full batteries (NVP||ETPTA–$NaClO_4$–QSSE||Na) display unprecedented rate capability, with a recorded capacity of 55 mAh g^{-1} at 15 C, higher than any achieved so far in solid-state SMBs, and long-term cycling stability at 5 C, offering a capacity retention of 97% after 1000 cycles. Furthermore, NVP||ETPTA–$NaClO_4$–QSSE||Na pouch cells represent excellent flexibility and exceptional safety, demonstrative of wide applicability. Therefore, this work will open new opportunities to develop room-temperature high-energy-density solid-state SMBs.

The growing demand for lithium-ion batteries (LIBs) has sparked fears of a potential Li shortage.[1–3] In order to achieve long-term development goal, low-cost alternative energy storage technologies are urgently needed. Sodium (Na) element has similar properties to Li, but is much more abundant and widely distributed, which make sodium-ion batteries (SIBs) a highly competitive alternative to LIBs.[4–6] However, the ionic radius of Na^+ is larger than Li^+, which is not suitable for the intercalation reaction of conventionally used graphite anode in LIBs. To this end, Na metal, with high theoretical capacity (1165 mAh g^{-1}) and a low redox potential (−2.71 V vs standard hydrogen potential) is regarded as an ideal anode material of SIBs with high output voltage and energy density.[1,5,7,8] Despite these advantageous features, sodium metal batteries (SMBs) in organic electrolyte systems still suffer from serious safety issues, such as the leakage of electrolyte, and dendrite formation of Na, which substantially inhibit the applicability of this type of battery.[7,9–11]

To overcome these safety issues, one promising and reliable strategy is to develop solid-state SMBs. This is because solid-state electrolytes can significantly bypass the risk of using flammable solvents, avoid the leakage of organic electrolyte, and importantly suppress the growth of dendrite.[10,12] However, the researchers still need to work through the downsides of solid-state electrolytes, such as low room-temperature ionic conductivity, high interfacial impedance, and narrow electrochemical window, before they can be commercially applied in practice.

So far, great efforts have been committed to the development and optimization of the solid-state electrolytes, including inorganic electrolytes and polymer electrolytes. The inorganic electrolytes, such as oxide solid-state electrolytes,[13–15] NASICON-type solid-state electrolytes,[16,17] and sulfide solid-state electrolytes,[18,19] usually present relatively good room-temperature ionic conductivity (>10^{-4} S cm^{-1}) and high mechanical strength. However, the solid–solid interface between inorganic electrolyte and electrode material usually exists high contact resistance. Furthermore, the rigid inorganic electrolytes appear poor

Dr. P. C. Wen, Dr. P. F. Lu, Dr. X. Y. Shi, H. D. Shi, H. Q. Liu, Prof. Z.-S. Wu
State Key Laboratory of Catalysis, Dalian Institute of Chemical Physics
Chinese Academy of Sciences
457 Zhongshan Road, Dalian 116023, China
E-mail: wuzs@dicp.ac.cn
Dr. Y. Yao, Prof. Y. Yu
Hefei National Laboratory for Physical Sciences at the Microscale
Department of Materials Science and Engineering
CAS Key Laboratory of Materials for Energy Conversion
University of Science and Technology of China
Hefei, Anhui 230026, China
H. D. Shi, H. Q. Liu
University of Chinese Academy of Sciences
19 A Yuquan Rd, Shijingshan District, Beijing 100049, China
Prof. Y. Yu, Prof. Z.-S. Wu
Dalian National Laboratory for Clean Energy
Chinese Academy of Sciences
457 Zhongshan Road, Dalian 116023, China

The ORCID identification number(s) for the author(s) of this article can be found under https://doi.org/10.1002/aenm.202002930.

DOI: 10.1002/aenm.202002930

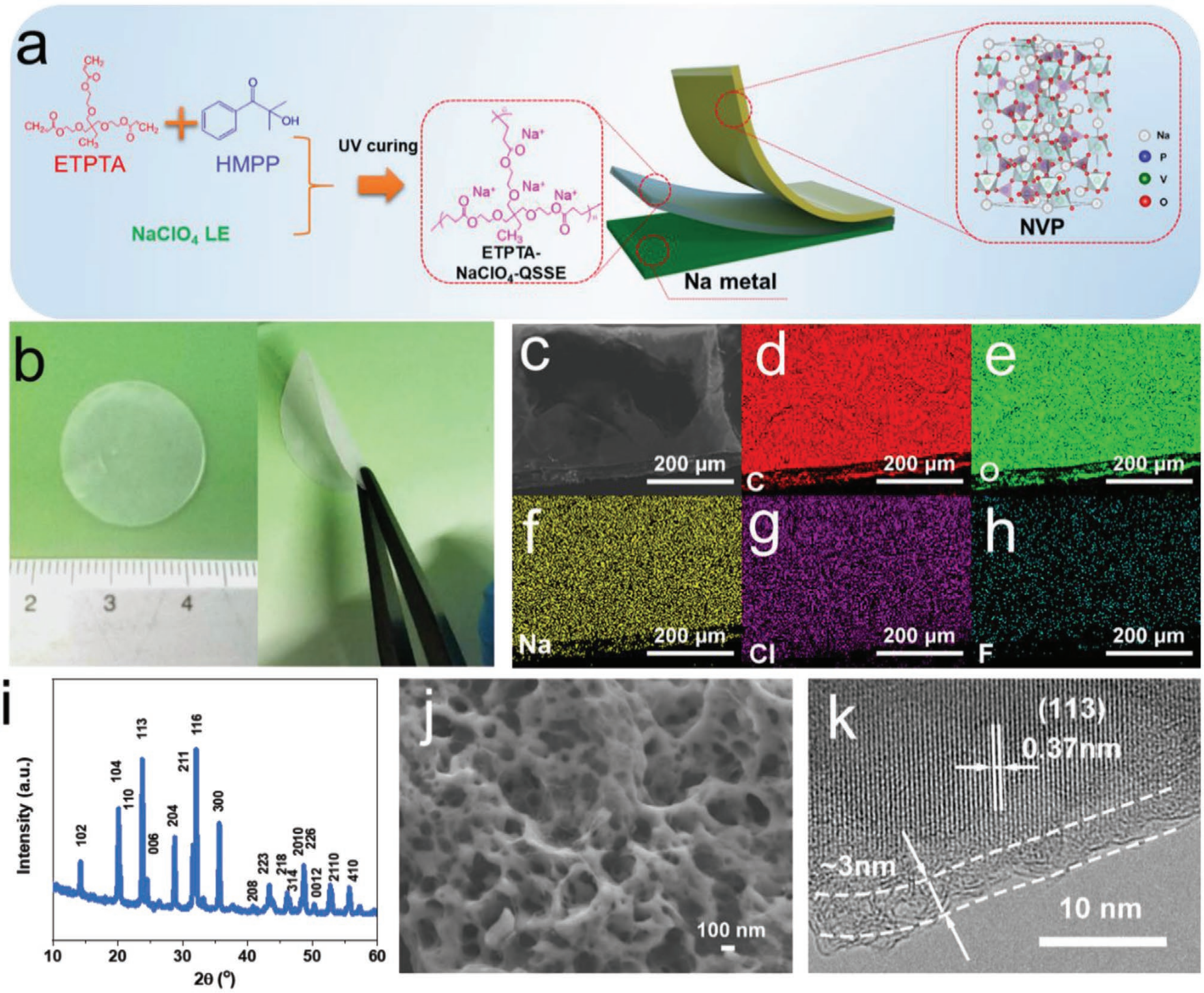

Figure 1. Fabrication and characterization of ETPTA–$NaClO_4$–QSSE, NVP, and NVP||ETPTA–$NaClO_4$–QSSE||Na SMBs. a) Schematic preparation of ETPTA–$NaClO_4$–QSSE and NVP||ETPTA–$NaClO_4$–QSSE||Na SMBs. b) Optical images of ETPTA–$NaClO_4$–QSSE membrane in a flat (left) and bent (right) states. c) SEM image and EDS element mappings d) C, e) O, f) Na, g) Cl, and h) F of ETPTA–$NaClO_4$–QSSE membrane. i) XRD pattern, j) SEM image, and k) HRTEM image of NVP.

toughness, which is not conducive to large-scale processability with low manufacturing cost. Besides, polymer electrolyte shows the advantages of excellent flexibility, easy processability, and exceptional interfacial contact with electrode, allowing for solid-state batteries with higher energy density and enhanced safety. Typically, polymer electrolyte is prepared by dissolving a Na salt, such as sodium perchlorate ($NaClO_4$), sodium bis(trifluoromethanesulfonyl) imide (NaTFSI), or sodium hexafluorophosphate ($NaPF_6$) in a polymer host, including polyethylene oxide (PEO),[20–22] poly(vinylidene fluoride-*co*-hexafluoropropylene) (PVDF–HFP),[23,24] poly(methyl methacrylate),[25,26] and polyacrylonitrile.[27,28] Owing to the excellent chemical stability and high solubility to Na salts, PEO-based electrolyte is considered to be the most promising electrolyte material.[12,22] However, PEO-based electrolyte appears limited mechanical properties, low oxidation potential, narrow voltage window (<4.0 V), and poor room-temperature ionic conductivity ($\approx 10^{-6}$ S cm^{-1}), which significantly limit their practical application for high-performance SMBs.[29–31]

To achieve high-energy-density solid-state SMBs, the cathode and anode also need to be matched accordingly. In a solid-state battery system, Na metal with high specific capacity can be used as anode, while solving the problems of poor electrode compatibility with solid-state electrolyte. For cathode, $Na_3V_2(PO_4)_3$ (NVP), with a high theoretical capacity of 117.6 mA g^{-1} and high output voltage of 3.4 V (vs Na^+/Na), which can approach an energy density of about 400 Wh kg^{-1}, is a key cathode material for sodium batteries.[32–34] However, pure NVP appears low electronic conductivity, and lacks of the efficient, low-cost preparation technology.[35,36] In addition, the interfacial optimization between the solid-state electrolyte and the electrode is crucial for constructing SMBs with superior performance. In this regard, polymer electrolytes have excellent flexibility to achieve better interface contact of electrolyte and

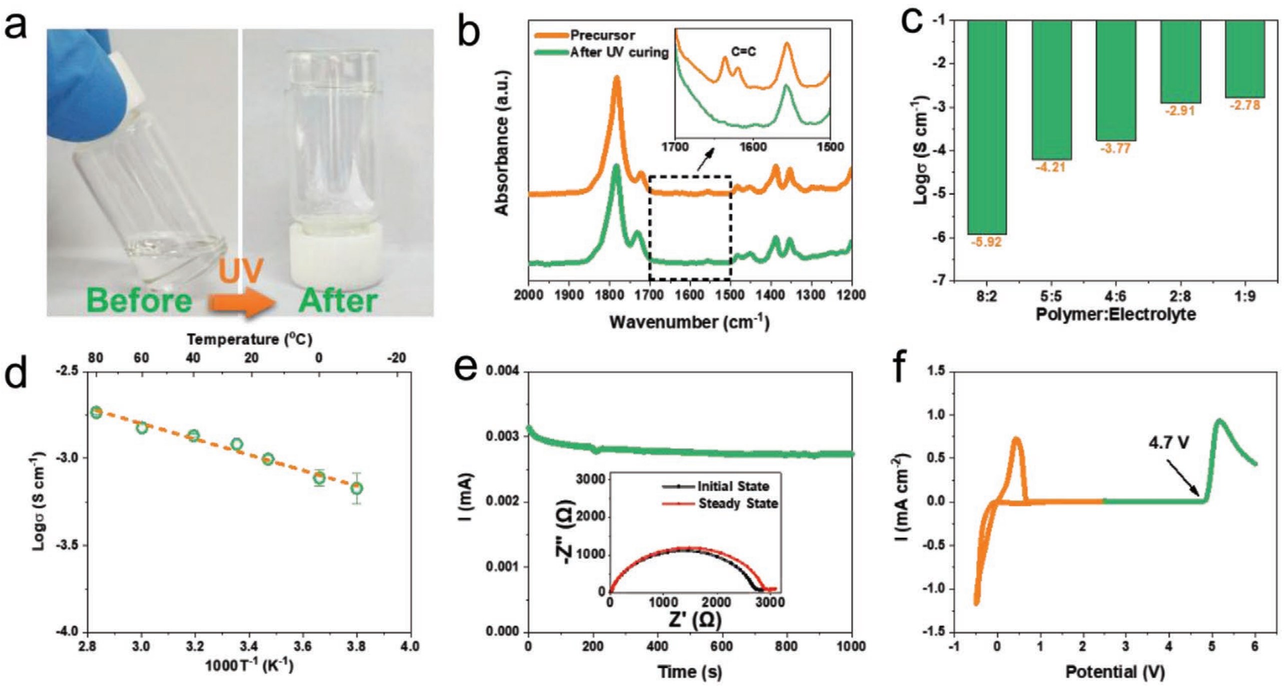

Figure 2. Characterization of ETPTA–$NaClO_4$–QSSE. a) Optical images and b) FTIR spectra of the gel electrolyte before and after UV curing. c) Room-temperature ionic conductivity of ETPTA–$NaClO_4$–QSSE with different polymer/electrolyte ratios. d) Ionic conductivity of ETPTA–$NaClO_4$–QSSE under varying temperature. e) Chronoamperometry for Na/ETPTA–$NaClO_4$–QSSE/Na cell at room temperature. Inset represents the Nyquist plots before and after polarization. f) CV and LSV curves of ETPTA–$NaClO_4$–QSSE.

electrode.[31,37,38] In addition, ultraviolet-curing polymers, such as ethoxylated trimethylolpropane triacrylate (ETPTA),[39–41] polyethylene glycol dimethacrylate (PEGDMA),[42,43] can obtain better interface contact and facilitate large-scale production of solid-state electrolyte membranes. For instance, Guo et al. reported a quasisolid-state poly(ethylene glycol) methyl ether acrylate (PEGMEA)-$LiPF_6$ electrolyte for lithium metal batteries, which can obtain ultraconformal interfacial contacts on the anode and cathode sides.[44] Nevertheless, developing high-energy-density solid-state SMBs with exceptionally matched electrode-electrolyte interface by a high room-temperature ionic conductive electrolyte still remains a great challenge.

Herein, a novel high ionic conductivity polymer, ETPTA-based quasisolid-state electrolyte (ETPTA–$NaClO_4$–QSSE), was prepared by photopolymerization for high-energy-density solid-state SMBs. The resulting ETPTA–$NaClO_4$–QSSE exhibits unprecedented room-temperature ionic conductivity of 1.2 mS cm^{-1}, and provides a wide electrochemical window up to 4.7 V (vs Na^+/Na) and extraordinary interfacial compatibility with Na metal anodes, effectively inhibiting the growth of Na dendrites. Moreover, the as-assembled solid-state SMBs (NVP||ETPTA–$NsaClO_4$–QSSE||Na) offer high specific capacity of 101 mAh g^{-1} at 1 C, and record rate performance (with a capacity of 55 mAh g^{-1} at high rate of 15 C) at room temperature that has been not yet achieved up to date. Further, the full battery of NVP||ETPTA–$NaClO_4$–QSSE||Na in pouch cell shows excellent flexibility and safety, demonstrative of wide applicability.

The fabrication of quasisolid-state electrolyte (ETPTA–$NaClO_4$–QSSE) and the assembly of solid-state SMBs (NVP||ETPTA–$NaClO_4$–QSSE||Na) are schematically shown in **Figure 1**a. First, the quasisolid-state electrolyte (ETPTA–$NaClO_4$–QSSE) is obtained by uniformly mixing the Na^+ electrolyte (1 м $NaClO_4$ in propylene carbonate and 5% fluoroethylene carbonate) into the photocuring agent ETPTA and 1% 2-hydroxy-2-methylpropiophenone (HMPP), then dropping it on a cellulose film and curing with ultraviolet light. As a result, a highly flexible ETPTA–$NaClO_4$–QSSE film, with a diameter of 19 mm, is obtained, which can be easily bent at sharp angle without any damage (Figure 1b). Scanning electron microscopy (SEM) image and energy dispersive X-ray spectroscopy (EDS) element mappings confirm the uniform distribution of C, O, Na, Cl, and F elements in ETPTA–$NaClO_4$–QSSE film (Figure 1c–h). Second, the carbon-coated NVP cathode representing typical NASICON structure (Figure 1i; and Figure S1a, Supporting Information) is prepared by a cost-effective sol–gel method.[33,45] SEM and transmission electron microscopy (TEM) images (Figure 1j; and Figure S1b, Supporting Information) present 3D interconnected porous structure, with a particle size of about 800 nm for NVP. High-resolution TEM (HRTEM) image (Figure 1k) displays the (113) plane of NVP, with *d*-spacing of 0.37 nm, and the existence of ultrathin carbon layer of 3 nm wrapped on the surface of NVP. Finally, the solid-state SMBs are constructed by using ETPTA–$NaClO_4$–QSSE film as both electrolyte and separator, carbon-coated NVP as cathode, and Na metal as anode.

The physical property of ETPTA–$NaClO_4$–QSSE was further studied after irradiating the fluid polymer precursor film by ultraviolet light for 20 s (**Figure 2**a). It can be observed that, after the irradiation, the Fourier-transform infrared spectroscopy (FTIR) characteristic peaks of the C=C bond at about

1610–1625 cm^{-1} are disappeared (Figure 2b), indicative of polymerization of ETPTA monomers.[40,43,46,47] X-ray diffraction (XRD) pattern only shows a broad peak at 20° (Figure S2, Supporting Information), proving the amorphous nature of photocured ETPTA–NaClO$_4$–QSSE. Thermogravimetric analysis of ETPTA–NaClO$_4$–QSSE electrolyte (Figure S3, Supporting Information) shows 5% weight loss at 159.9 °C, greater than that of liquid electrolyte (5% weight loss at 123.8 °C), indicative of impressive thermal stability of ETPTA–NaClO$_4$–QSSE.

The room-temperature ionic conductivity of ETPTA–NaClO$_4$–QSSE with different (ETPTA+HMPP)/NaClO$_4$ electrolyte ratios (e.g., 8: 2, 5: 5, 4: 6, 2: 8, 1: 9) were systematically compared in Figure 2c. It is revealed that the ionic conductivity of the electrolyte increases with increased content of electrolyte. Notably, the room-temperature ionic conductivity of ETPTA–NaClO$_4$–QSSE is higher than 1.2 mS cm^{-1} when the polymer/electrolyte ratio is less than 2:8. With polymer/electrolyte ratio of 1:9, the ionic conductivity increases to 1.6 mS cm^{-1}. However, this gel electrolyte cannot be cured well, even for prolonging irradiation time to 2 min. Further, it is observed that the tensile strength of ETPTA–NaClO$_4$–QSSE membrane gradually weakens with the increasing content of electrolyte, and the tensile strength of electrolyte with polymer/electrolyte ratio of 1:9 is greatly reduced compared to that with a ratio of 2:8 (Figure S4, Supporting Information). Therefore, an optimal polymer/electrolyte ratio is chosen to be 2:8 by balancing the ionic conductivity and mechanical property. Furthermore, the ionic conductivity of ETPTA–NaClO$_4$–QSSE was measured at different temperatures (Figure 2d). It is observed that the quasisolid-state electrolyte shows increased ionic conductivity with increasing temperature, for example, 0.7, 0.8, 1.0, 1.2, 1.4, 1.5, and 1.8 mS cm^{-1} are obtained at –10, 0, 15, 25, 40, 60, and 80 °C, respectively, suggestive of excellent temperature adaptability. It is worth noting that such high room-temperature ionic conductivity of 1.2 mS cm^{-1} (25 °C) outperforms the currently reported sodium-based PEO solid-state electrolytes (about 10^{-6} S cm^{-1}).[29–31,48] Moreover, the standard deviation of room-temperature ionic conductivity of ETPTA–NaClO$_4$–QSSE is only 0.058, manifesting the repeated properties of the electrolyte.

The Na$^+$ transference number (t_{Na^+}) can reflect the dissociative Na$^+$ in ETPTA–NaClO$_4$–QSSE.[49,50] Therefore, the value of t_{Na^+} was evaluated before and after polarization under 10 mV in AC impedance measurement at room temperature (Figure 2e), in which the intermediate frequency semicircle of the impedance spectra are closely related to the interface resistance between Na metal and ETPTA–NaClO$_4$–QSSE. It is calculated that the value of t_{Na^+} is 0.62, bigger than the most PEO-based solid-state electrolytes (usually < 0.4).[49–51] This is likely attributed to the fact that the polymerized ETPTA framework greatly restricts the movement of anions, and the larger movement space and rotation space of the polymer segment are beneficial for the transportation of Na$^+$.[43] In order to understand the movement rule of Na$^+$ and ClO$_4^-$, the first-principles density functional theory calculations were performed to probe the migration energy barrier of Na$^+$ and ClO$_4^-$ in the ETPTA polymer chain (Figure S5, Supporting Information). It is calculated that the migration energy barrier of Na$^+$ in ETPTA polymer segments is only 0.1 eV, while that of ClO$_4^-$ is as high as 0.8 eV. This result shows that Na$^+$ is easier to move between polymer segments, and the higher migration energy of ClO$_4^-$ leads to greatly restricted migration in polymer segments. Further, cyclic voltammetry (CV) and linear sweep voltammetry (LSV) curves are carried out, as shown in Figure 2f. Apparently, the redox/oxidation peaks at –0.5/0.5 V are assigned to Na plating/stripping.[43] It can be seen that the ETPTA–NaClO$_4$–QSSE exhibits the stability down to 0 V (vs Na$^+$/Na) in the cathodic scan, indicative of exceptional electrochemical interface with Na metal. In addition, the LSV of ETPTA–NaClO$_4$–QSSE shows significantly stable electrochemical window up to 4.7 V versus Na$^+$/Na, demonstrative of high voltage stability.

To evaluate the electrochemical compatibility and dynamic stability of interface between ETPTA–NaClO$_4$–QSSE and Na metal, the symmetrical cells of Na||ETPTA–NaClO$_4$–QSSE||Na were assembled, and their voltage profiles pertaining to Na plating/stripping at a current density of 0.1 mA cm^{-2} for 1 h were measured (**Figure 3**a). The inset figures are the enlarged voltage profiles of 200–204, 500–504, and 996–1000 h. It is found that the symmetrical cell has an ultralow overpotential of only 70 mV, and exhibits extremely stable cycling performance without any fluctuation for 1000 h. Further, it is disclosed that the overpotential of the symmetry cell decreases gradually in the initial stage and becomes stable in the subsequent cycles. It can be explained by electrochemical impedance spectroscopy (EIS) (Figure S6, Supporting Information) that shows a decreasing trend of charge transfer resistance, due to the gradually enhanced contact of Na metal and electrolyte over the charging and discharging process.

To highlight the importance of ETPTA–NaClO$_4$–QSSE, the rate performance of Na||ETPTA–NaClO$_4$–QSSE||Na symmetrical cell was measured at different current densities for 15 min in the Na stripping and plating processes (Figure 3b; and Figure S7, Supporting Information). Impressively, it is revealed that the overpotentials of Na||ETPTA–NaClO$_4$–QSSE||Na symmetrical cells are only 70, 151, 232, 254, 310, and 355 mV with increasing current densities of 0.1, 0.2, 0.4, 0.6, 0.8, and 1 mA cm^{-2}, respectively. Notably, the maximum withstand current density of ETPTA–NaClO$_4$–QSSE is much higher than those of recently reported works, such as PEO-based electrolyte (0.1 mA cm^{-2}),[37,52] $Na_3Zr_2Si_2PO_{12}$ (0.25 mA cm^{-2}),[16–53] Na_3SbS_4 (0.1 mA cm^{-2}),[54,55] Na_2S–P_2S_5 (0.013 mA cm^{-2}),[56] thermoplastic polyurethane-based electrolyte (0.5 mA cm^{-2}),[57] PVDF–HFP based electrolyte (0.5 mA cm^{-2})[58] (Table S1, Supporting Information). Furthermore, such low overpotential can be readily restored to 64 mV after the current density reduces back to 0.1 mA cm^{-2}, suggestive of excellent rate capability. Therefore, the outstanding performance of Na||ETPTA–NaClO$_4$–QSSE||Na symmetrical cells demonstrates exceptionally matched interface compatibility of ETPTA–NaClO$_4$–QSSE with Na metal anode, effectively inhibiting the growth of Na dendrites, and improving the stability of Na anode.

In order to further probe the effect of electrolytes on the dendrite growth of Na metal, a Na–Na symmetrical battery was built to perform the in situ observation on the changes on the surface of Na metal during charge and discharge under optical microscope (Figure 3c,d), tested at current density of 0.1 mA cm^{-2}. In the case of pure liquid electrolyte-based Na–Na symmetrical battery (denoted as Na||LE||Na), it is apparently observed that a large amount of gas bubbles are released in the discharging process,

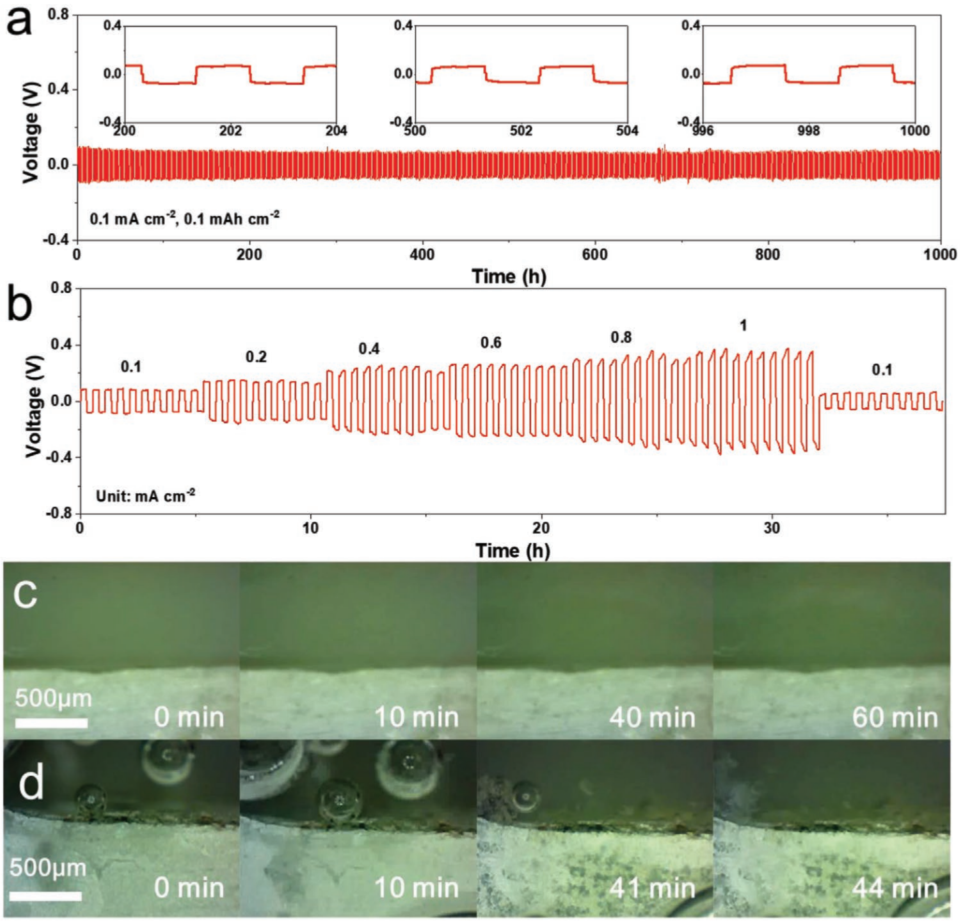

Figure 3. Electrochemical characterization of Na||ETPTA–NaClO$_4$–QSSE||Na symmetrical batteries. a) Voltage profile of Na||ETPTA–NaClO$_4$–QSSE||Na symmetrical battery plating/stripping at 0.1 mA cm^{-2} for 1 h. Insets are the enlarged voltage profiles of 200–204, 500–504, and 996–1000 h. b) Voltage profiles of Na||ETPTA–NaClO$_4$–QSSE||Na symmetrical battery plating/stripping at 0.1, 0.2, 0.4, 0.6, 0.8, 1, and 0.1 mA cm^{-2} for 15 min. c,d) In situ observation of Na electrodeposition process in the c) Na||ETPTA–NaClO$_4$–QSSE||Na and d) Na||LE||Na symmetrical battery under optical microscope.

accompanied by the appearance of dendrite and formation of dead Na on the surface of Na metal after depositing 41 min. In fact, the dendrite grows rapidly within a short period of time, about 3 min, and partly falls off to form dead sodium (Figure 3d). On a sharp contrast, it can be seen that with the extension of the plating time, there is no obvious growth of the dendrite on the surface of Na metal in the Na||ETPTA–NaClO$_4$–QSSE||Na battery. It is demonstrated that the quasisolid-state electrolyte can effectively suppress the formation of Na dendrite, endowing outstanding stability and safety of SMBs.

To demonstrate the superiority of ETPTA–NaClO$_4$–QSSE, the solid-state full batteries of NVP||ETPTA–NaClO$_4$–QSSE||Na are assembled with NVP cathode, Na metal anode, and quasisolid-state electrolyte (**Figure 4**). For comparison, the pure liquid electrolyte-based NVP||LE||Na batteries are also fabricated. It is revealed that galvanostatic charge and discharge profiles (Figure 4a) of NVP||ETPTA–NaClO$_4$–QSSE||Na battery exhibits a two-phase reaction mechanism,[42] and low polarization voltages approximately of 0.20, 0.24, 0.33, 0.39, 0.44, 0.49, and 0.62 V at different rates of 1, 2, 4, 6, 8, 10, and 15 C, respectively. Notably, NVP||ETPTA–NaClO$_4$–QSSE||Na battery shows unprecedented rate performance, which can maintain high average capacities of 103 mAh g^{-1} at 1 C, 88 mAh g^{-1} at 6 C, and 55 mAh g^{-1} at 15 C (Figure 4b). Furthermore, the capacity can be restored to 102 mAh g^{-1}, when the rate goes back to 1 C. Importantly, Ragone plot (Figure 4c) reveals high energy density of 334 W h kg^{-1} and power density of 5411 W kg^{-1} (based on NVP mass in cathode) for NVP||ETPTA–NaClO$_4$–QSSE||Na batteries, indicative of wide applicability. It should be emphasized that such high rate capability (55 mAh g^{-1} at 15 C) are superior to the state-of-the-art solid-state SMBs, which has been not achieved up to date (Figure 4d; and Table S2, Supporting Information).[38,48,52,59–70]

Further, the NVP||ETPTA–NaClO$_4$–QSSE||Na battery showcases exceptional long-term cycling stability compared with the NVP||LE||Na battery (Figure 4e). Although both have similar initial discharge capacity (about 102 mAh g^{-1}) of NVP||ETPTA–NaClO$_4$–QSSE||Na and NVP||LE||Na at 1 C, the discharge capacity of the latter decreases fast to 60 mAh g^{-1} after 1000 cycles, and capacity retention is only 59% (Figure 4e; and Figure S8a, Supporting Information). Impressively, NVP||ETPTA–NaClO$_4$–QSSE||Na batteries provide a significantly high discharge capacity of 98 mAh g^{-1} after 1000 cycles, with a high capacity retention of 96% (Figure 4e; and Figure S8b,

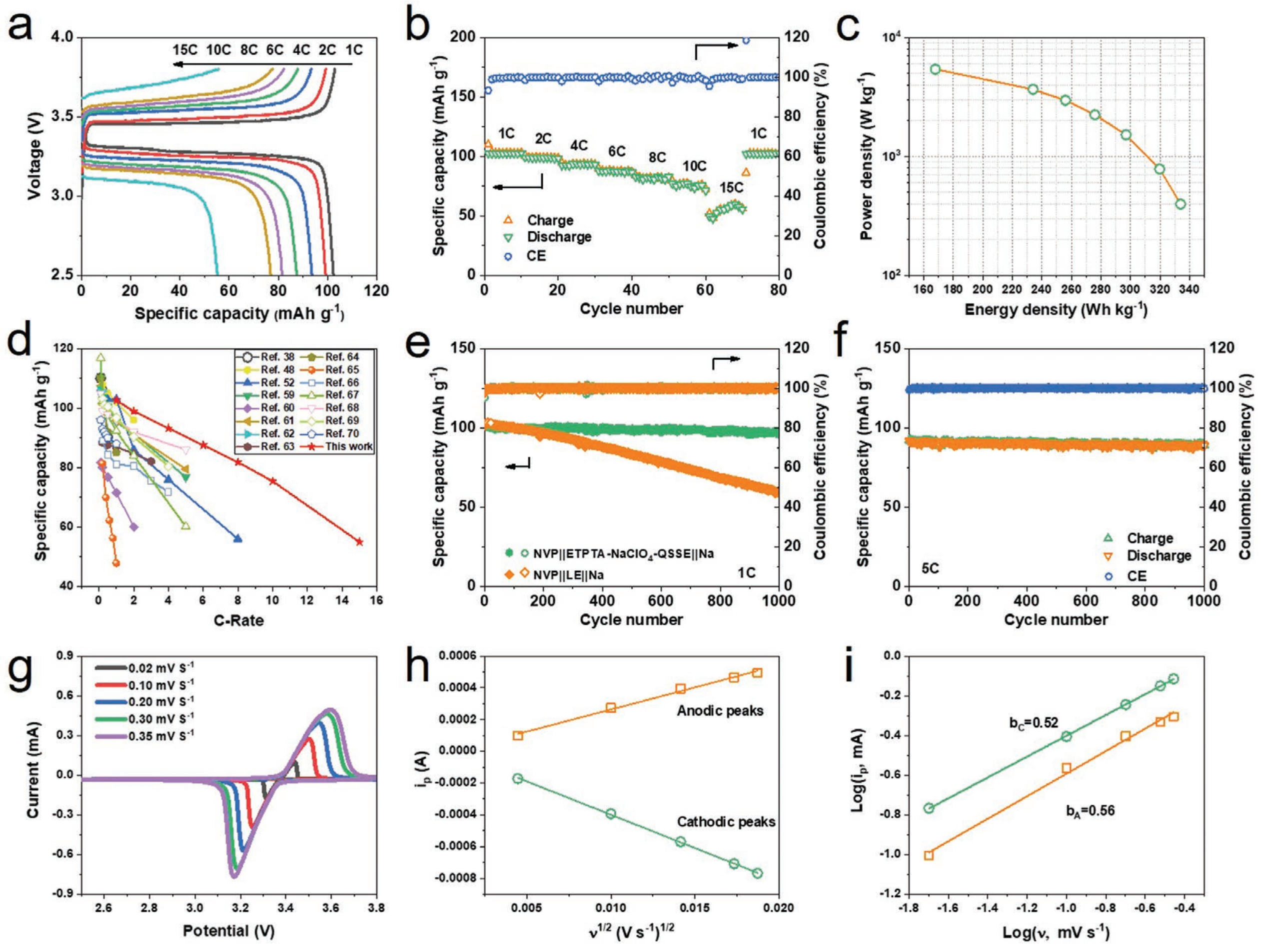

Figure 4. Electrochemical performance of NVP||ETPTA–NaClO$_4$–QSSE||Na SMBs. a) Galvanostatic charge and discharge profiles obtained at different rates, b) Rate performance, and c) Ragone plot of NVP||ETPTA–NaClO$_4$–QSSE||Na SMBs. d) Comparison of electrochemical performance of NVP||ETPTA–NaClO$_4$–QSSE||Na SMBs with the reported NVP based SMBs. e) Cycling stability of NVP||ETPTA–NaClO$_4$–QSSE||Na battery and NVP||LE||Na battery measured at 1 C. f) Cycle performance of NVP||ETPTA–NaClO$_4$–QSSE||Na battery obtained at 5 C. g) CV curves of NVP||ETPTA–NaClO$_4$–QSSE||Na battery tested at various sweep rates. h) The linear fitting plots of i_p versus $v^{1/2}$. i) The linear fitting plots of log(i_p) versus log(v).

Supporting Information). It is worth noting that the two discharge platforms of NVP||ETPTA–NaClO$_4$–QSSE||Na battery in the initial cycles are probably due to a local redox environment rearrangement from the transfer of Na (1) to Na (2) commonly found in NASICON materials.[71,72] By comparing EIS spectra at the 50th and 100th cycle of these two batteries (Figure S9, Supporting Information), it is uncoiled that the internal impedance of NVP||LE||Na battery increases from 126 Ω at 50th cycle to 178 Ω at 100th cycle, owing to the gradual growth of dendrites and formation of dead Na in liquid system as the cycle progresses. In contrast, NVP||ETPTA–NaClO$_4$–QSSE||Na battery can keep the stable internal resistance at the 50th and 100th cycle, suggestive of key role of ETPTA–NaClO$_4$–QSSE on the improvement of cycling stability. As demonstrated, even the rate increases to 5 C (Figure 4f), NVP||ETPTA–NaClO$_4$–QSSE||Na battery still offers high initial discharge capacity of 92 mAh g^{-1}, and maintains 97% of initial capacity after 1000 cycles with high Coulombic efficiency of more than 99.9%.

To validate the fast electrochemical kinetics, the CV curves of NVP||ETPTA–NaClO$_4$–QSSE||Na SMBs were tested at different scan rates from 0.02 to 0.35 mV s^{-1} (Figure 4g). It is observed that the polarization of NVP||ETPTA–NaClO$_4$–QSSE||Na is as small as 0.13 V at 0.02 mV s^{-1}, manifesting outstanding ion migration performance. Further, the negligible shift of ≈0.15 V in the cathodic/anodic pair from 0.02 to 0.35 mV s^{-1} further demonstrates the fast kinetics of NVP||ETPTA–NaClO$_4$–QSSE||Na battery. The diffusion coefficient of Na$^+$ (D_{Na}) is an important kinetic index, which is calculated by the Randles–Sevcik equation (Equation (1)).[73,74]

$$i_p = 2.69 \times 10^5 n^{3/2} A D_{Na}^{1/2} C_{Na} v^{1/2} \tag{1}$$

Where D_{Na} is diffusion coefficient of Na$^+$, i_p is the peak current (A), n is the number of transferred electrons, A is the surface area of the electrode, C_{Na} is the concentration of Na$^+$, and v is the scan rate. According to the linear fitting plots of i_p versus $v^{1/2}$, the diffusion coefficient D_{Na} of anodic peaks and cathodic peaks is calculated as 4.32 × 10^{-11} and 9.78 × 10^{-11} cm^2 s^{-1}. Therefore, it is evidenced that Na$^+$ ions possess the ability of fast diffusion in NVP||ETPTA–NaClO$_4$–QSSE||Na battery.

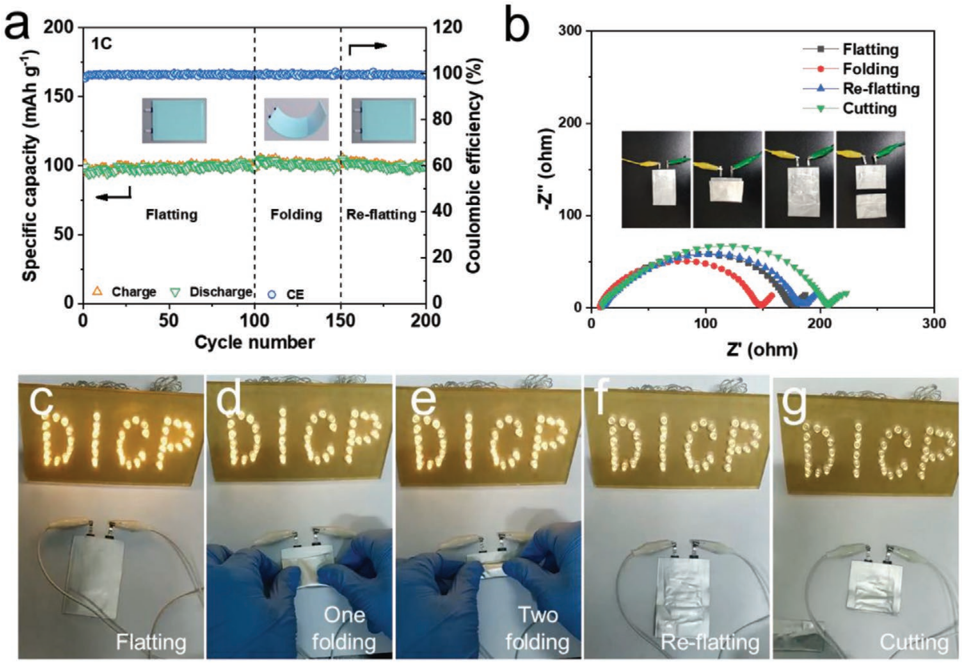

Figure 5. Electrochemical and safety performance of NVP||ETPTA–NaClO$_4$–QSSE||Na pouch cells. a) Cycling stability of the pouch cell tested at 1 C. b) Nyquist plots of the pouch cell tested in the flatting, folding, reflatting and cutting states. c–g) The destructive condition test of NVP||ETPTA–NaClO$_4$–QSSE||Na pouch cell in the c) flatting, d) one folding, e) two folding, f) reflatting, and g) cutting states.

The i_p and v also obey the power law $i = av^b$, where a and b are adjustable parameters, and the b value is used to determine the type of electrochemical reaction (diffusion control or/and surface control mechanism). When the b value is closer to 1, it means that the capacitive behavior accounts for a higher proportion and the reaction kinetics is faster. According to the linear fitting plots of log(i_p) versus log(v), b values for anodic peaks (b_A) and cathodic peaks (b_C) are calculated to be 0.56 and 0.52, respectively, suggesting fast reaction kinetics of NVP||ETPTA–NaClO$_4$–QSSE||Na battery.

To validate the real application of ETPTA–NaClO$_4$–QSSE in flexible electronics, the cycling performance of NVP||ETPTA–NaClO$_4$–QSSE||Na pouch cell was measured in flatting state, folding state, and reflatting state, respectively (**Figure 5**a) at 1 C at room temperature. Remarkably, NVP||ETPTA–NaClO$_4$–QSSE||Na pouch cell exhibits high reversible discharge capacity of ≈100 mAh g^{-1} at 1 C after the first 100 cycles. Furthermore, it can still maintain a stable reversible capacity of ≈100 mAh g^{-1} even if the cell is cycled in the subsequent 50 cycles under folding state (from 101th to 150th cycle) and another 50 cycles under reflatting state (from 151th to 200th cycle). It should be mentioned that there is no leakage or short circuit in this battery, and the EIS just have only minor changes in different states (Figure 5b). The EIS tested under folded state shows slightly reduced impedance, which is possibly caused by the intimate contact of cathode, anode, and ETPTA–NaClO$_4$–QSSE for the enhancement of interface interaction. To confirm the key protective effect of ETPTA–NaClO$_4$–QSSE on Na metal anode, this solid-state battery was cut to proof the reliability and safety. Significantly, after cutting, the impedance of the battery increases slightly (about 50 Ω) as the penetration of air that causes a slight oxidation of Na metal (Figure S10, Supporting Information), this solid-state SMB is inflammable yet highly stable. Even after cutting for 1 h, the impedance only increased by about 50 Ω, and the open-circuit voltage decreased by about 0.8 V without short circuit occurred. Moreover, the destructive condition tests were further performed on the flexible NVP||ETPTA–NaClO$_4$–QSSE||Na battery (Figure 5c–g). After charging NVP||ETPTA–NaClO$_4$–QSSE||Na battery with 25% state of charge, the flatting state battery can light up 42 light emitting diodes (LEDs). Also, for the one folding, two folding, reflatting, and cutting test, this battery still keeps the LED light on. Therefore, it is proved that the NVP||ETPTA–NaClO$_4$–QSSE||Na pouch cell has remarkable flexibility and safety performance under complex working conditions.

In summary, we developed a new photopolymerized quasisolid-state electrolyte of ETPTA–NaClO$_4$–QSSE for high-energy-density and stable SMBs. The ETPTA–NaClO$_4$–QSSE displays unprecedented room-temperature ionic conductivity of 1.2 mS cm^{-1}, a wide electrochemical window up to 4.7 V (vs Na$^+$/Na), and outstanding compatibility with Na metal anode for significantly inhibiting the formation of Na dendrites. Owing to the high room-temperature ionic conductivity of ETPTA–NaClO$_4$–QSSE with enhanced interfacial protection of Na metal anode, the NVP||ETPTA–NaClO$_4$–QSSE||Na batteries show superior rate performance and long-term cycling stability, maintaining a record reversible discharge capacity of 55 mAh g^{-1} at 15 C, and 97% capacity retention after 1000 cycles at 5 C. Importantly, NVP||ETPTA–NaClO$_4$–QSSE||Na pouch cell displays excellent flexibility and safety performance. Therefore, this strategy proposed for quasisolid-state electrolyte provides a new direction for the development of room-temperature high-energy-density flexible solid-state SMBs.

Supporting Information

Supporting Information is available from the Wiley Online Library or from the author.

Acknowledgements

The authors acknowledge the financial support from National Key R&D Program of China (Grant Nos. 2016YBF0100100 and 2016YFA0200200), National Natural Science Foundation of China (Grant Nos. 51872283, 21805273, 51925207, 51872277, and U1910210), Liaoning BaiQianWan Talents Program, LiaoNing Revitalization Talents Program (Grant No. XLYC1807153), Natural Science Foundation of Liaoning Province, Joint Research Fund Liaoning-Shenyang National Laboratory for Materials Science (Grant No. 20180510038), DICP (Nos. DICP ZZBS201708, DICP ZZBS201802, and DICP I202032), DICP&QIBEBT (Grant No. DICP&QIBEBT UN201702), Dalian National Laboratory For Clean Energy (DNL), CAS, DNL Cooperation Fund, CAS (Nos. DNL180310, DNL180308, DNL201912, and DNL201915), and the Fundamental Research Funds for the Central Universities (No. WK2060140026).

Conflict of Interest

The authors declare no conflict of interest.

Keywords

high energy density, photopolymerized gel electrolytes, sodium metal anodes, sodium metal batteries, solid state

Received: September 14, 2020
Revised: October 15, 2020

---

[1] M. D. Slater, D. Kim, E. Lee, C. S. Johnson, *Adv. Funct. Mater.* **2013**, *23*, 947.
[2] K. Chayambuka, G. Mulder, D. L. Danilov, P. H. Notten, *Adv. Energy Mater.* **2018**, *8*, 1800079.
[3] H. L. Pan, Y. S. Hu, L. Q. Chen, *Energy Environ. Sci.* **2013**, *6*, 2338.
[4] W. Luo, C. F. Lin, O. Zhao, M. Noked, Y. Zhang, G. W. Rubloff, L. B. Hu, *Adv. Energy Mater.* **2017**, *7*, 1601526.
[5] H. Wang, C. Wang, E. Matios, W. Li, *Angew. Chem., Int. Ed.* **2018**, *57*, 7734.
[6] Y. Zhao, X. Yang, L. Y. Kuo, P. Kaghazchi, Q. Sun, J. Liang, B. Wang, A. Lushington, R. Li, H. Zhang, *Small* **2018**, *14*, 1703717.
[7] B. Sun, P. Li, J. Zhang, D. Wang, P. Munroe, C. Wang, P. H. L. Notten, G. Wang, *Adv. Mater.* **2018**, *30*, 1801334.
[8] C. Zhao, Y. Lu, J. Yue, D. Pan, Y. Qi, Y.-S. Hu, L. Chen, *J. Energy Chem.* **2018**, *27*, 1584.
[9] Y. Sun, P. Shi, H. Xiang, X. Liang, Y. Yu, *Small* **2019**, *15*, 1805479.
[10] Q. L. Ma, M. Guin, S. Naqash, C. L. Tsai, F. Tietz, O. Guillon, *Chem. Mater.* **2016**, *28*, 4821.
[11] X. Zheng, H. Fu, C. Hu, H. Xu, Y. Huang, J. Wen, H. Sun, W. Luo, Y. Huang, *J. Phys. Chem. Lett.* **2019**, *10*, 707.
[12] C. Zhao, L. Liu, X. Qi, Y. Lu, F. Wu, J. Zhao, Y. Yu, Y.-S. Hu, L. Chen, *Adv. Energy Mater.* **2018**, *8*, 1703012.
[13] K. B. Hueso, M. Armand, T. Rojo, *Energy Environ. Sci.* **2013**, *6*, 734.
[14] X. Lu, G. Li, J. Y. Kim, J. P. Lemmon, V. L. Sprenkle, Z. Yang, *J. Power Sources* **2012**, *215*, 288.
[15] J.-J. Kim, K. Yoon, I. Park, K. Kang, *Small Methods* **2017**, *1*, 1700219.
[16] W. Zhou, Y. Li, S. Xin, J. B. Goodenough, *ACS Cent. Sci.* **2017**, *3*, 52.
[17] Z. Zhang, Q. Zhang, J. Shi, Y. S. Chu, X. Yu, K. Xu, M. Ge, H. Yan, W. Li, L. Gu, Y.-S. Hu, H. Li, X.-Q. Yang, L. Chen, X. Huang, *Adv. Energy Mater.* **2017**, *7*, 1601196.
[18] N. J. J. de Klerk, M. Wagemaker, *Chem. Mater.* **2016**, *28*, 3122.
[19] A. Hayashi, K. Noi, A. Sakuda, M. Tatsumisago, *Nat. Commun.* **2012**, *3*, 856.
[20] G. Chen, Y. Bai, Y. Gao, Z. Wang, K. Zhang, Q. Ni, F. Wu, H. Xu, C. Wu, *ACS Appl. Mater. Interfaces* **2019**, *11*, 43252.
[21] J.-F. Wu, Z.-Y. Yu, Q. Wang, X. Guo, *Energy Storage Mater.* **2020**, *24*, 467.
[22] Q. Ma, J. Liu, X. Qi, X. Rong, Y. Shao, W. Feng, J. Nie, Y.-S. Hu, H. Li, X. Huang, L. Chen, Z. Zhou, *J. Mater. Chem. A* **2017**, *5*, 7738.
[23] H. Gao, B. Guo, J. Song, K. Park, J. B. Goodenough, *Adv. Energy Mater.* **2015**, *5*, 1402235.
[24] J. I. Kim, Y. Choi, K. Y. Chung, J. H. Park, *Adv. Funct. Mater.* **2017**, *27*, 1701768.
[25] H. Gao, W. Zhou, K. Park, J. B. Goodenough, *Adv. Energy Mater.* **2016**, *6*, 1600467.
[26] D. Kumar, S. A. Hashmi, *J. Power Sources* **2010**, *195*, 5101.
[27] Z. Osman, K. B. M. Isa, A. Ahmad, L. Othman, *Ionics* **2010**, *16*, 431.
[28] K. Vignarooban, P. Badami, M. A. K. L. Dissanayake, P. Ravirajan, A. M. Kannan, *Ionics* **2017**, *23*, 2817.
[29] S. R. Mohapatra, A. K. Thakur, R. N. P. Choudhary, *Ionics* **2008**, *14*, 255.
[30] J. S. Moreno, M. Armand, M. B. Berman, S. G. Greenbaum, B. Scrosati, S. Panero, *J. Power Sources* **2014**, *248*, 695.
[31] A. Boschin, P. J. E. A. Johansson, *Electrochim. Acta* **2015**, *175*, 124.
[32] Y. Jiang, X. Zhou, D. Li, X. Cheng, F. Liu, Y. Yu, *Adv. Energy Mater.* **2018**.
[33] S. Tao, P. Cui, W. Huang, Z. Yu, X. Wang, S. Wei, D. Liu, L. Song, W. Chu, *Carbon* **2016**, *96*, 1028.
[34] X. Zhang, X. Rui, D. Chen, H. Tan, D. Yang, S. Huang, Y. Yu, *Nanoscale* **2019**, *11*, 2556.
[35] W. Duan, Z. Zhu, H. Li, Z. Hu, K. Zhang, F. Cheng, J. Chen, *J. Mater. Chem. A* **2014**, *2*, 8668.
[36] J. Liu, K. Tang, K. Song, P. A. van Aken, Y. Yu, J. Maier, *Nanoscale* **2014**, *6*, 5081.
[37] X. Xu, Y. Li, J. Cheng, G. Hou, X. Nie, Q. Ai, L. Dai, J. Feng, L. Ci, *J. Energy Chem.* **2020**, *41*, 73.
[38] Z. Zhang, K. Xu, X. Rong, Y.-S. Hu, H. Li, X. Huang, L. Chen, *J. Power Sources* **2017**, *372*, 270.
[39] K.-H. Choi, S.-J. Cho, S.-H. Kim, Y. H. Kwon, J. Y. Kim, S.-Y. Lee, *Adv. Funct. Mater.* **2014**, *24*, 44.
[40] E.-H. Kil, K.-H. Choi, H.-J. Ha, S. Xu, J. A. Rogers, M. R. Kim, Y.-G. Lee, K. M. Kim, K. Y. Cho, S.-Y. Lee, *Adv. Mater.* **2013**, *25*, 1395.
[41] W. Fan, N.-W. Li, X. Zhang, S. Zhao, R. Cao, Y. Yin, Y. Xing, J. Wang, Y.-G. Guo, C. Li, *Adv. Sci.* **2018**, *5*, 1800559.
[42] Y. Yao, Z. Wei, H. Wang, H. Huang, Y. Jiang, X. Wu, X. Yao, Z. S. Wu, Y. Yu, *Adv. Energy Mater.* **2020**, *10*, 1903698.
[43] Z. Wei, Z. Zhang, S. Chen, Z. Wang, X. Yao, Y. Deng, X. Xu, *Energy Storage Mater.* **2019**, *22*, 337.
[44] Z. Li, X.-Y. Zhou, X. Guo, *Energy Storage Mater.* **2020**, *29*, 149.
[45] S.-h. Luo, J.-y. Li, S. Bao, Y.-y. Liu, Z. Wang, *J. Electrochem. Soc.* **2018**, *165*, E563.
[46] H.-J. Ha, Y. H. Kwon, J. Y. Kim, S.-Y. Lee, *Electrochim. Acta* **2011**, *57*, 40.
[47] H. J. Ha, E. H. Kil, Y. H. Kwon, J. Y. Kim, C. K. Lee, S. Y. Lee, *Energy Environ. Sci.* **2012**, *5*, 6491.
[48] R. T. Gao, R. Tan, L. Han, Y. Zhao, Z. J. Wang, L. Y. Yang, F. Pan, *J. Mater. Chem. A* **2017**, *5*, 5273.
[49] T. Zhu, X. Dong, Y. Liu, Y.-G. Wang, C. Wang, Y.-Y. Xia, *ACS Appl. Energy Mater.* **2019**, *2*, 5263.
[50] Q. Ma, J. J. Liu, X. G. Qi, X. H. Rong, Y. J. Shao, W. F. Feng, J. Nie, Y. S. Hu, H. Li, X. J. Huang, L. Q. Chen, Z. B. Zhou, *J. Mater. Chem. A* **2017**, *5*, 7738.
[51] X. G. Qi, Q. Ma, L. L. Liu, Y. S. Hu, H. Li, Z. B. Zhou, X. J. Huang, L. Q. Chen, *ChemElectroChem* **2016**, *3*, 1741.

[52] C. Ma, K. Dai, H. Hou, X. Ji, L. Chen, D. G. Ivey, W. Wei, *Adv. Sci.* **2018**, *5*, 1700996.

[53] W. Niu, L. Chen, Y. Liu, L.-Z. Fan, *Chem. Eng. J.* **2020**, *384*, 123233.

[54] P. Hu, Y. Zhang, X. Chi, K. K. Rao, F. Hao, H. Dong, F. Guo, Y. Ren, L. C. Grabow, Y. Yao, *ACS Appl. Mater. Interfaces* **2019**, *11*, 9672.

[55] Y. S. Tian, Y. Z. Sun, D. C. Hannah, Y. H. Xiao, H. Liu, K. W. Chapman, S. H. Bo, G. Ceder, *Joule* **2019**, *3*, 1037.

[56] K. Noi, A. Hayashi, M. Tatsumisago, *J. Power Sources* **2014**, *269*, 260.

[57] M.-S. Park, H.-S. Woo, J.-M. Heo, J.-M. Kim, R. Thangavel, Y.-S. Lee, D.-W. Kim, *ChemSusChem* **2019**, *12*, 4645.

[58] Y.-J. Kim, H. Lee, H. Noh, J. Lee, S. Kim, M.-H. Ryou, Y. M. Lee, H.-T. Kim, *ACS Appl. Mater. Interfaces* **2017**, *9*, 6000.

[59] L. L. Liu, X. G. Qi, S. J. Yin, Q. Q. Zhang, X. Z. Liu, L. M. Suo, H. Li, L. Q. Chen, Y. S. Hu, *ACS Energy Lett.* **2019**, *4*, 1650.

[60] T. C. Mendes, X. M. Zhang, Y. T. Wu, P. C. Howlet, M. Forsyth, D. R. Macfarlane, *ACS Sustainable Chem. Eng.* **2019**, *7*, 3722.

[61] Q. P. Yu, Q. W. Lu, X. G. Qi, S. Y. Zhao, Y. B. He, L. L. Liu, J. Li, D. Zhou, Y. S. Hu, Q. H. Yang, F. Y. Kang, B. H. Li, *Energy Storage Mater.* **2019**, *23*, 610.

[62] Z. Z. Zhang, Q. Q. Zhang, C. Ren, F. Luo, Q. Ma, Y. S. Hu, Z. B. Zhou, H. Li, X. J. Huang, L. Q. Chen, *J. Mater. Chem. A* **2016**, *4*, 15823.

[63] J. F. Yang, M. Zhang, Z. Chen, X. F. Du, S. Q. Huang, B. Tang, T. T. Dong, H. Wu, Z. Yu, J. J. Zhang, G. L. Cui, *Nano Res.* **2019**, *12*, 2230.

[64] X. J. Zhang, X. C. Wang, S. Liu, Z. L. Tao, J. Chen, *Nano Res.* **2018**, *11*, 6244.

[65] Q. Y. Pan, Z. Li, W. C. Zhang, D. L. Zeng, Y. B. Sun, H. S. Cheng, *Solid State Ionics* **2017**, *300*, 60.

[66] P. Wang, H. R. Zhang, J. C. Chai, T. M. Liu, R. X. Hu, Z. H. Zhang, G. C. Li, G. L. Cui, *Solid State Ionics* **2019**, *337*, 140.

[67] Y. Gao, G. Chen, X. Wang, H. Yang, Z. Wang, W. Lin, H. Xu, Y. Bai, C. Wu, *ACS Appl. Mater. Interfaces* **2020**, *12*, 22981.

[68] D. Lei, Y.-B. He, H. Huang, Y. Yuan, G. Zhong, Q. Zhao, X. Hao, D. Zhang, C. Lai, S. Zhang, J. Ma, Y. Wei, Q. Yu, W. Lv, Y. Yu, B. Li, Q.-H. Yang, Y. Yang, J. Lu, F. Kang, *Nat. Commun.* **2019**, *10*, 4244.

[69] Y. Lu, J. A. Alonso, Q. Yi, L. Lu, Z. L. Wang, C. Sun, *Adv. Energy Mater.* **2019**, *9*, 1901205.

[70] T. Lan, C.-L. Tsai, F. Tietz, X.-K. Wei, M. Heggen, R. E. Dunin-Borkowski, R. Wang, Y. Xiao, Q. Ma, O. Guillon, *Nano Energy* **2019**, *65*, 104040.

[71] P. Feng, W. Wang, K. Wang, S. Cheng, K. Jiang, *J. Mater. Chem. A* **2017**, *5*, 10261.

[72] X. Jiang, L. Yang, B. Ding, B. Qu, G. Ji, J. Y. Lee, *J. Mater. Chem. A* **2016**, *4*, 14669.

[73] Y. Xiao, Y.-F. Zhu, H.-R. Yao, P.-F. Wang, X.-D. Zhang, H. Li, X. Yang, L. Gu, Y.-C. Li, T. Wang, Y.-X. Yin, X.-D. Guo, B.-H. Zhong, Y.-G. Guo, *Adv. Energy Mater.* **2019**, *9*, 1803978.

[74] J.-Z. Guo, P.-F. Wang, X.-L. Wu, X.-H. Zhang, Q. Yan, H. Chen, J.-P. Zhang, Y.-G. Guo, *Adv. Mater.* **2017**, *29*, 1701968.